Translational Diffusion of Bovine Prothrombin Fragment 1 Weakly Bound to Supported Planar Membranes: Measurement by Total Internal Reflection with Fluorescence Pattern Photobleaching Recovery

Zhengping Huang, Kenneth H. Pearce, and Nancy L. Thompson
Department of Chemistry, University of North Carolina at Chapel Hill, Chapel Hill, North Carolina 27599-3290 USA

ABSTRACT Previous work has shown that bovine prothrombin fragment 1 binds to substrate-supported planar membranes composed of phosphatidylcholine (PC) and phosphatidylserine (PS) in a Ca^{2+}-specific manner. The apparent equilibrium dissociation constant is 1–15 μM, and the average membrane residency time is $\approx 0.25\ s^{-1}$. In the present work, fluorescence pattern photobleaching recovery with evanescent interference patterns (TIR-FPPR) has been used to measure the translational diffusion coefficients of the weakly bound fragment 1. The results show that the translational diffusion coefficients on fluid-like PS/PC planar membranes are on the order of 10^{-9} cm^2/s and are reduced when the fragment 1 surface density is increased. Control measurements were carried out for fragment 1 on solid-like PS/PC planar membranes. The dissociation kinetics were similar to those on fluid-like membranes, but protein translational mobility was not detected. TIR-FPPR was also used to measure the diffusion coefficient of the fluorescent lipid NBD-PC in fluid-like PS/PC planar membranes. In these measurements, the diffusion coefficient was $\approx 10^{-8}$ cm^2/s, which is consistent with that measured by conventional fluorescence pattern photobleaching recovery. This work represents the first measurement of a translational diffusion coefficient for a protein weakly bound to a membrane surface.

INTRODUCTION

The membrane-mediated conversion of prothrombin to thrombin is a key process in thrombosis and hemostasis. This reaction also serves as a paradigm for several enzymatic processes in blood coagulation that require the association of proteins containing γ-carboxyglutamic acid residues with membranes that contain negatively charged phospholipids (such as platelet surfaces). Of particular interest is how transport and reaction are coupled at the membrane surface during the assembly of the prothrombinase enzyme complex and during subsequent prothrombin cleavage (Mann et al., 1990; Jackson and Nemerson, 1980; Abbott and Nelsestuen, 1988).

One method for obtaining quantitative information about the physical dynamics of proteins at membrane surfaces is to use substrate-supported planar membranes and techniques in fluorescence microscopy (Thompson et al., 1993a, b, 1994). Previous work has shown that bovine prothrombin and its fragment 1 weakly bind to supported membranes composed of mixtures of palmitoyloleoylphosphatidylcholine (POPC) and bovine brain phosphatidylserine (PS) in a Ca^{2+}-specific manner and that fluorescence microscopy can be used to measure both equilibrium and kinetic rate constants for membrane binding (Tendian et al., 1991; Pearce et al., 1992, 1993). In addition, the bound fragment 1 reduces the diffusion coefficient of fluorescent phospholipids in the planar membranes (Huang et al., 1992).

A physical parameter that has not been readily measurable for proteins weakly bound to membrane surfaces is the translational diffusion coefficient. As described herein, one method for directly measuring the translational diffusion coefficients of proteins reversibly bound to substrate-supported membrane surfaces is to use evanescent interference patterns with fluorescence pattern photobleaching recovery (TIR-FPPR) (Abney et al., 1992; Huang and Thompson, 1993). In this method, two internally reflected laser beams are collided to create a periodic evanescent intensity pattern that illuminates a region of a solid/liquid interface. For fluorescently labeled molecules that are weakly bound to the surface and in equilibrium with the solution, the fluorescence recovery after photobleaching contains information about the kinetic association/dissociation rates and the surface diffusion coefficient.

TIR-FPPR has previously been used to examine fluorescently labeled IgE in the contact region between rat basophil leukemia cells and supported planar membranes (Weis et al., 1982); bovine serum albumin adsorbed to artificial surfaces (Tilton et al., 1990a, b); phospholipid vesicles at supported planar membrane surfaces (Kalb et al., 1992); and organic polymers at various interfaces (Miehlich and Gaub, 1993). Here TIR-FPPR was used to measure the translational diffusion coefficient of bovine prothrombin fragment 1 weakly bound to supported planar membranes in its Ca^{2+}- and phosphatidylserine-specific manner. This work represents the first measurement of a translational diffusion coefficient for a protein that is weakly bound to a phospholipid membrane surface.

Received for publication 28 April 1994 and in final form 27 July 1994.

Address reprint requests to Dr. Nancy L. Thompson, Department of Chemistry, University of North Carolina, CB #3290, Chapel Hill, NC 27599-3290. Tel.: 919-962-0328; Fax: 919-962-2388; E-mail: thompson@uncvx1.oit.unc.edu.

Dr. Pearce's present address: Department of Protein Engineering, Genentech, Inc., South San Francisco, CA 94080.

0006-3495/94/10/1754/13 $2.00

MATERIALS AND METHODS

Reagents

Bovine prothrombin fragment 1 was purified from bovine plasma and labeled with fluorescein isothiocyanate (Molecular Probes, Inc., Eugene, OR) as previously described (Pearce et al., 1992). The concentrations of labeled proteins were determined by the bicinchonic acid assay (Pierce Chemical Co., Rockford, IL), and the molar ratios of fluorescein to protein (0.6–1.6) were determined using the molar absorptivity of protein-conjugated fluorescein at 494 nm (ϵ = 64,800 M^{-1} cm^{-1}; Molecular Probes). Fragment 1 was stored in Tris-buffered saline (TBS; 0.05 M Tris, 0.1 M NaCl, pH 7.4) at −20°C until use. Bovine brain phosphatidylserine (PS), 1-palmitoyl-2-oleoyl-3-*sn*-phosphatidylcholine (POPC), 1-acyl-2-[12-[(7-nitro-2,1,3-benzoxadiazol-4-yl)-amino]dodecanoyl]-phosphatidylcholine (NBD-PC), 1,1-dipalmitoyl-*sn*-glycero-3-[phospho-L-serine] (DPPS), 1,2-dipalmitoyl-*sn*-glycero-3-phosphocholine (DPPC), and 1,2-dipalmitoyl-*sn*-glycero-3-phosphoethanolamine-*N*-(7-nitro-2–1,3-benzoxadiazol-4-yl) (NBD-DPPE) were obtained commercially (Avanti Polar Lipids, Birmingham, AL) and used without further purification.

Planar membranes

Substrate-supported planar membranes were constructed by depositing small unilamellar vesicles on 1" × 1" × 1 mm fused silica substrates as described previously (Pearce et al., 1992). Vesicles were prepared at 2 mM either from PS and POPC, or DPPS and DPPC, by sonication and ultracentrifugation. For measurements of lipid translational mobility, 2 mol% NBD-PC was incorporated in PS/POPC (10/88 mol/mol) vesicles or 2 mol% NBD-DPPE was incorporated in DPPS/DPPC (10/88 mol/mol) vesicles. Vesicles were fused and deposited on substrates by spontaneous adsorption for 25 min followed by rinsing with 2 ml TBS. Planar membranes were then treated with 250 μl of TBS containing various concentrations of unlabeled fragment 1, fluorescein-labeled fragment 1, 10 mM $CaCl_2$, or 1 mM Na_2EDTA. Samples containing fragment 1 were prepared so that labeled fragment 1 was diluted 10-fold by unlabeled fragment 1 to yield the appropriate final concentration. All 250-μl samples were incubated at room temperature for 25 min before use.

TIR-FPPR instrumentation

Fig. 1 illustrates the optical elements of the experimental apparatus. The fluorescence microscope was composed of an argon ion laser (Innova 90–3, Coherent Inc., Palo Alto, CA; without etalon), an inverted optical microscope (Zeiss IM-35, Eastern Microscope Co., Raleigh, NC), and a single-photon-counting photomultiplier (C31034A, RCA, Lancaster, PA) interfaced to an IBM PC AT computer (Pearce et al., 1992). The laser beam first entered a device that consisted of two 10/90 beam splitters and two mirrors to select between high and low laser intensities for photobleaching and fluorescence monitoring, respectively. A neutral density filter (ND1) further lowered the monitoring beam intensity. Two computer-controlled shutters were used to select the bleaching (intense) and observation (dim) beams. The bleaching and observation beams were split into two parallel beams using a 50/50 beam splitter and a mirror (M). A neutral density filter (ND2) was inserted to adjust the beams to equal intensity, and three mirrors (PLC) were inserted to compensate for the pathlength difference. The two parallel beams passed through a lens with a large focal length (LS1; 232 mm) and a lens with a smaller focusing length (LS2). The distance between the two parallel beams was controlled by using lenses LS2 with different focal lengths (25, 50, 75, 100, 150, or 175 mm). The two s-polarized beams were directed through a final focusing lens (LS3; focal length 75 mm) and a cubic quartz prism [(1.5 cm)^3] and interfered at the point of internal reflection. The instrument was judged to be properly aligned when fringes were seen in focus through the microscope (Fig. 2). Fringe pattern periods were varied by changing the intersection angle (2ϕ) using LS2. The apparatus was mounted on a vibration isolation table to eliminate fringe fluctuations; the position of the fringes was stable over time and appeared to be identical within optical resolution for both the bleaching and observation beams. Evanescently excited fluorescence was collected through a microscope objective and directed through a barrier filter (B) and an aperture (A) to the photomultiplier. The aperture was adjusted so that the photomultiplier viewed ≈10–15 fringes. Control data were collected by blocking one of the two interfering beams and increasing the laser power twofold.

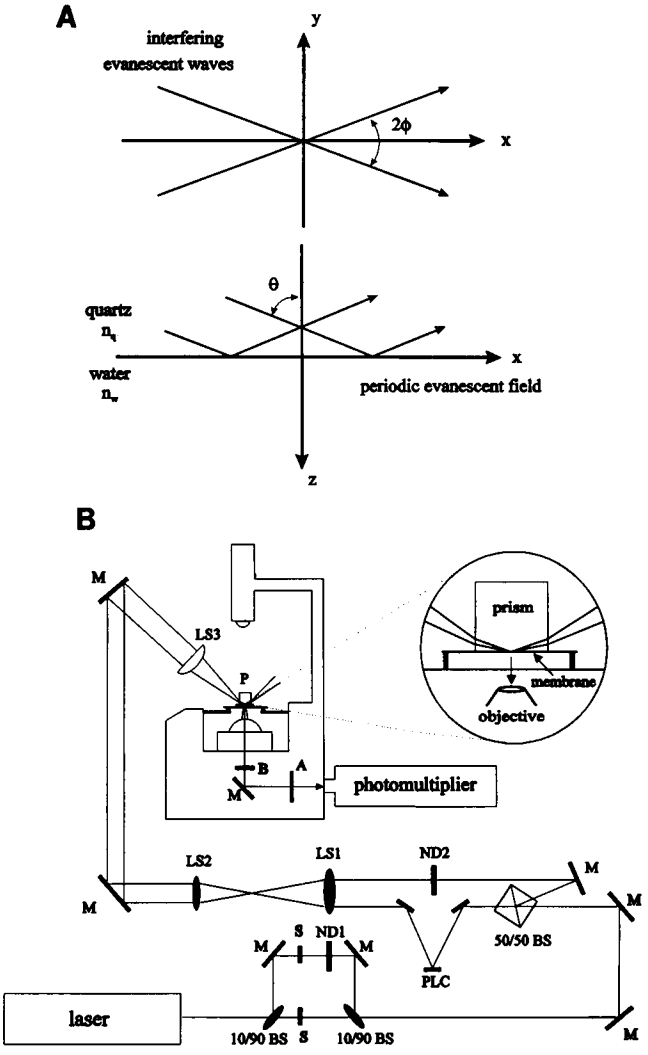

FIGURE 1 Schematic of the optical arrangement for TIR-FPPR. (*A*) Two laser beams are totally internally reflected at a planar interface between quartz and water. The interface is defined as the *x-y* plane with the *x* axis bisecting the two incidence planes. The incidence angle for the two beams is θ, and the angle between the two incidence planes is 2ϕ. (*B*) Two 10/90 beam splitters (BS) are used to create beams of relatively high and low intensities for bleaching and observation, respectively. A neutral density filter (ND1) is used to reduce further the observation beam intensity. Two shutters (S) are used to control both the bleaching and observation beams. Two parallel beams are generated by a 50/50 beam splitter and a mirror (M). Three mirrors (PLC) are inserted to compensate for the pathlength difference. A neutral density filter (ND2) is used to adjust the intensity difference. Two lenses (LS1, LS2) are used to vary the intersection angle 2ϕ. The two converging beams enter the prism (P) through a focusing lens (LS3) and interfere at the point of internal reflection, generating an evanescent field with a sinusoidally varying intensity. Fluorescence is collected through the microscope objective and directed through a barrier filter (B) and an aperture (A) to a detector.

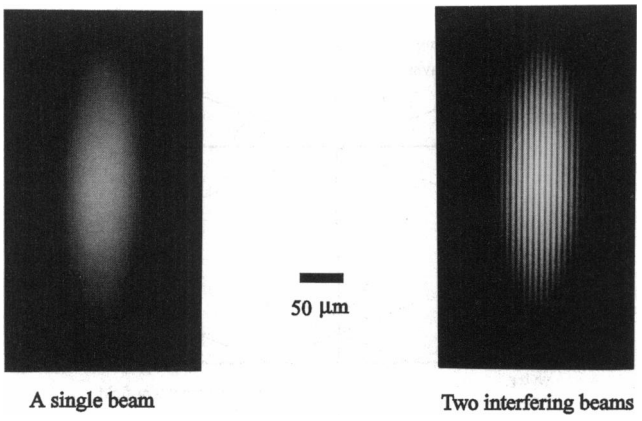

FIGURE 2 Experimental evanescent fields. Evanescent fields were created by totally internally reflecting an argon ion laser beam through a quartz prism: (*A*) a single beam; (*B*) two interfering beams.

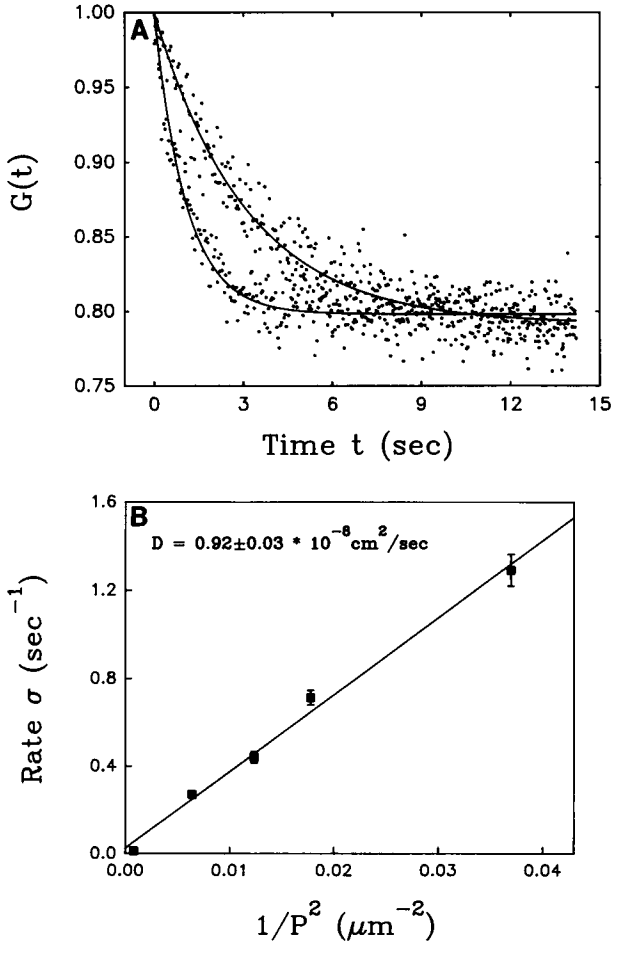

FIGURE 3 TIR-FPPR Data for NBD-PC in PS/POPC Planar Membranes. (*A*) Shown are typical curves for NBD-PC/PS/POPC bilayers with pattern periods 12.5 μm (*top*) and 7 μm (*bottom*). Decreasing the pattern period increases the rate of fluorescence recovery. The lines show the best fits to Eqs. 1 and 2. (*B*) The values of rate σ, obtained from the best fits of data like those in *A* to Eqs. 1 and 2, are plotted as a function of $1/P^2$, where *P* is the fringe pattern period. The error bars at each point are SDs of the means. The slope of the best fit to a line predicts the diffusion coefficient. The uncertainty in the diffusion coefficient was calculated using linear regression

Measurement of translational mobilities

The translational mobilities of NBD-PC in PS/POPC planar membranes and of fluorescein-labeled fragment 1 on both PS/POPC and DPPS/DPPC planar membranes were measured with TIR-FPPR. Parameters were as follows: laser wavelength, 488.0 nm; objective, Zeiss, 40X, 0.75 N.A.; observation laser power, 20–50 μW; bleaching laser power, 0.5 W; bleaching pulse duration, 20–60 ms; depth of bleaching, 70–75%; incidence angles θ, 75°; fringe pattern period, 4–15 μm; length of the short axis of the elliptically illuminated area, 50–200 μm; observed area, 10–15 fringes.

In some control measurements, the translational mobilities of NBD-PC in PS/POPC planar membranes and of NBD-DPPE on DPPS/DPPC planar membranes were measured with conventional fluorescence pattern photobleaching recovery (FPPR; Smith and McConnell, 1978) as previously described (Wright et al., 1988). Parameters were as follows: laser wavelength, 488.0 nm; objective, Zeiss, 40X, 0.75 N.A.; observation laser power, 5–10 μW; bleaching laser power, 0.5 W; bleaching pulse duration, 200–500 ms; depth of bleaching, 60–80%; ruling periodicity in the sample plane, 16 μm; radii of illuminated and observed areas, ≥90 and 75 μm, respectively.

Recovery curves were fit to theoretical forms for the fluorescence recovery, $F(t)$, using the nonlinear curve-fitting routine in ASYST (Macmillan Software, New York, NY). Data and their best fits are plotted as

$$G(t) = \frac{F(-) - F(t)}{F(-) - F(0)}, \quad (1)$$

where $F(0)$ is the fluorescence immediately after photobleaching and $F(-)$ is the fluorescence before photobleaching.

RESULTS AND DISCUSSION

Lipid diffusion measured by FPPR

The translational mobility of 2 mol% NBD-PC in fluid-like planar membranes consisting of PS/POPC (10/88 mol/mol) was measured by conventional FPPR (Smith and McConnell, 1978; Wright et al., 1988; Huang et al., 1992). The measured diffusion coefficient was $(1.15 \pm 0.09) \times 10^{-8}$ cm²/s, and the fractional mobility was 0.78 ± 0.03. Similar measurements were carried out on solid-like planar membranes consisting of DPPS/DPPC (10/88 mol/mol) with 2 mol% NBD-DPPE as the fluorescent probe. These measurements indicated that the lipid translational diffusion coefficient in the solid-like membranes was $<10^{-10}$ cm²/s.

Lipid diffusion measured by TIR-FPPR

In control measurements, the translational diffusion of NBD-PC in PS/POPC planar membranes was examined using TIR-FPPR. In this case, the fluorescent lipids remained bound to the surface and the fluorescence recovery resulted only from translational diffusion along the interface. As shown in Fig. 3 *A*, the characteristic time for fluorescence recovery was on the order of seconds and increased with the pattern period.

As shown in Appendix A, the shape of the fluorescence recovery for a single diffusing component irreversibly adsorbed to the surface is described by

$$G(t) = (1 - h) + he^{-\sigma t} \quad (2)$$

where

$$\sigma = \beta^2 D \tag{3a}$$

$$\beta = \frac{2\pi}{P} \tag{3b}$$

$$h = \frac{Z_1(\eta, V)}{1 + Z_1(\eta, V) - Z_0(\eta, V)} \approx \frac{V^2}{2 + V^2} \tag{3c}$$

$$Z_i(\eta, V) = V^i e^{-\eta} I_i(\eta, V). \tag{3d}$$

D is the diffusion coefficient, P is the period of the evanescent interference pattern, η is a parameter proportional to the bleaching intensity and duration (Eq. A7), V is the visibility (or contrast) of the interference pattern, I_0 and I_1 are modified Bessel functions, and the approximation holds in the limit of shallow bleaching.

TIR-FPPR data were fit to Eqs. 1 and 2 with $F(-)$ fixed at the known value and $F(0)$, h, and σ as free parameters. The rates σ were plotted versus $1/P^2$, and these data were fit by linear regression (Fig. 3 *B*). The resultant straight line confirmed the diffusive mechanism of the translational mobility. The slope of the line yields a lipid translational diffusion coefficient of $D = (0.92 \pm 0.03) \times 10^{-8}$ cm^2/s, which is consistent with that measured by conventional FPPR (see above).

Fractional recovery in lipid diffusion measurements

The rate of fluorescence recovery is determined by the surface diffusion coefficient D and the pattern period P in both conventional FPPR and TIR-FPPR. However, although the maximum fractional recovery R (Eq. B1a) and change C (Eq. B1b) do not depend on the bleaching depth B (Eq. B1c) in conventional FPPR, the relationship among R, C, and B is not straightforward in TIR-FPPR (Abney et al., 1992; Huang and Thompson, 1993). As described in Appendix B,

$$R = h \tag{4a}$$

$$C = Z_1(\eta, V) \tag{4b}$$

$$B = 1 - Z_0(\eta, V) + Z_1(\eta, V), \tag{4c}$$

where V is the visibility (Eq. A1c), η is a bleaching parameter (Eq. A7), and the Z_i are defined in Eq. 3d.

Fig. 4 *A* shows the predicted values of R (Eq. 4a) as a function of the bleaching parameter η and the visibility V. As shown, R is in general lower for deeper bleaching depths (increasing η) and for imperfect contrast ($V < 1$). The average fractional recovery for NBD-PC in PS/POPC membranes, measured by TIR-FPPR, was $R = 0.19 \pm 0.02$, and the average fractional bleach was $B = 0.73 \pm 0.02$. The low value of R is an intrinsic feature of TIR-FPPR. For a bleaching depth $B = 0.73$ ($\eta = 1$), the maximum theoretical value of R is 0.28 ($V = 1$). Given that the fractional mobility is ≈0.78 (see above), the measured value of R agrees reasonably well with its predicted value ($0.78 \times 0.28 = 0.22$).

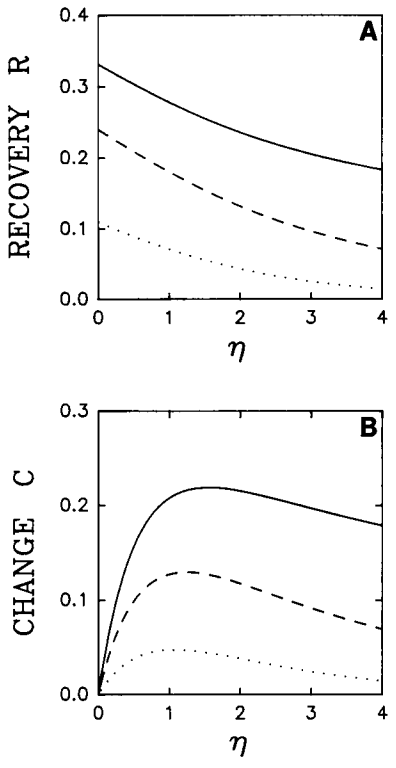

FIGURE 4 The fractional recovery R and fractional fluorescence change C, as functions of the bleaching parameter η and the visibility V. Values of R and C were calculated using Eqs. 3, c and d, and 4, a and b; they are shown for $V = 1$ (——), $V = 0.8$ (– – –), and $V = 0.5$ (· · · ·). The parameters V and η are defined in Eqs. A1c and A7, respectively. (*A*) R is lower for deeper bleaching depths and for imperfect contrast ($V < 1$). (*B*) The maximum value of C is 0.22 and occurs for $\eta \approx 1.5$ and $V = 1$, corresponding to $B = 0.8$.

The precision of diffusion coefficients measured with TIR-FPPR is related more closely to the average fractional fluorescence change C than to the fractional fluorescence recovery R. For example, although the recovery R is maximized in the limit of very low bleaching, TIR-FPPR data are noisy in this limit because the net fluorescence change is small. The values of C calculated from Eq. 4b are shown in Fig. 4 *B* for different values of η and V. The maximum value of C is ≈ 0.22 and occurs for $V = 1$, $\eta = 1.5$, and $B = 0.8$. The measured value of C for NBD-PC in PS/POPC planar membranes was $C = 0.14 \pm 0.02$.

A possible explanation for the low measured values of R and C is that the bleaching and observation beam interference patterns were shifted in phase. As shown in Appendix B, for a phase shift of ξ,

$$C = Z_1(\eta, V)\cos(\xi) \tag{5a}$$

$$B = 1 - Z_0(\eta, V) + Z_1(\eta, V)\cos(\xi). \tag{5b}$$

and R is given by Eqs. 5a, 5b, and B1a.

Fig. 5 shows the dependence of R, C, and B on the phase shift ξ and bleaching parameter η. All three parameters decrease with $\xi > 0$, and R and C are negative for $\xi > \pi/2$. Experimentally, $B \approx 0.73$ and $V \approx 1$. When adjusted for the incomplete mobility (≈ 0.78) as measured by FPPR, the

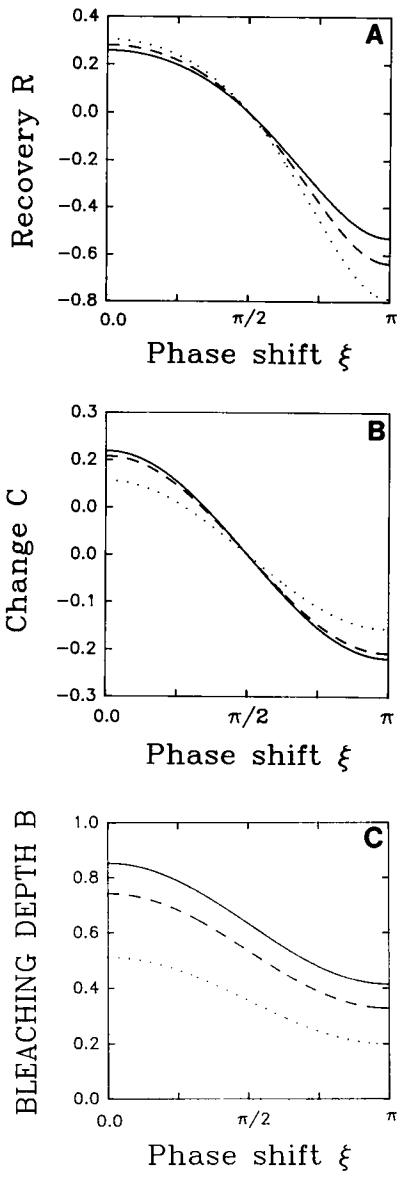

FIGURE 5 The fractional recovery R, the fractional fluorescence change C, and the bleaching depth B, as functions of the phase shift ξ and of the bleaching parameter η. Values of (A) R, (B) C, and (C) B were calculated using Eqs. 5 and B1a and are shown for $V = 1$ and $\eta = 1.5$ (——), $\eta = 1.0$ (– – –), or $\eta = 0.5$ (· · · ·). The parameters V, η, and ξ are defined in Eqs. A1c, A7, and B2, respectively. B decreases with ξ. Both R and C are maximized when $\xi = 0$, minimized when $\xi = \pi$, and zero when $\xi = \pi/2$.

measured values of R and C are $R \approx 0.24$ and $C \approx 0.18$. Therefore, if a phase shift between the bleaching and observation interference patterns is the explanation for the low measured values of R and C, Eqs. 5 and B1a predict that $\xi \approx 33°$ (given $V = 1$). Phase shifts between the bleaching and observation beams would be caused by shifts in the relative phase of the two interfering beams (Abney et al., 1992). The optical resolution was not high enough for phase shifts of this magnitude to be visually apparent.

A different explanation for the low measured values of R and C is that the bleaching process is not a single exponential as a function of the bleaching intensity and duration (Eq. A5). As shown in Appendix B for biexponential bleaching (Eq. B4)

$$C = bZ_1(\eta_1, V) + (1 - b)Z_1(\eta_2, V) \quad (6a)$$

$$B = 1 - [bZ_0(\eta_1, V) + (1 - b)Z_0(\eta_2, V)] + [bZ_1(\eta_1, V) + (1 - b)Z_1(\eta_2, V)] \quad (6b)$$

where b is the relative amplitude of the first bleaching process and the Z_i are defined in Eq. 3d. R is given by Eqs. 6a, 6b, and B1a.

Fig. 6 shows the dependence of R, C and B on η_1 and η_2. In these plots, it has been assumed for simplicity that $V = 1$ and $b = 0.5$. In this case, B increases for higher values of η_1 and η_2, whereas R and C have maxima at intermediate values of η_1 and η_2. The maximum value of $C \approx 0.22$ occurs when $\eta_1 \approx \eta_2 \approx 1.5$. The maximum value of $R \approx 0.33$ occurs when η_1 and η_2 approach zero. Both R and C are linear with the parameter b, and their maxima with respect to this parameter, for given values of η_1 and η_2, occur for $b = 0$ or $b = 1$, which corresponds to a single exponential bleaching process. By using the biexponential model as the explanation for the low measured values of R and C, the assumptions that $V = 1$ and $b = 0.5$, the measured value of B, and the measured and adjusted values of R and C (see above), one finds that Eqs. 6 and B1a predict that $Z_0(\eta_1, V) + Z_0(\eta_2, V) = 0.90$ and $Z_1(\eta_1, V) + Z_1(\eta_2, V) = 0.36$. The predicted values of these two sums imply that $\eta_1 = 0.5$ and $\eta_2 = 2.7$.

Protein binding specificity

The previously published (Pearce et al., 1993) equilibrium binding curve for fragment 1 on PS/POPC (10/90 mol/mol) planar membranes was reproduced, except that bovine serum albumin (BSA) was not included (data not shown). Binding curves were constructed by measuring the evanescently excited fluorescence of fragment 1 on PS/POPC (10/90 mol/mol) planar membranes as a function of the fragment 1 solution concentration. All samples contained 10 mM Ca^{2+} except for the control samples, which contained 1 mM EDTA. Although BSA was previously included to block possible nonspecific binding, it was not used in the measurements described herein because of its potential to block or retard the translational motion of the bound fragment 1 or lipids adsorbed to the substrates. The apparent equilibrium dissociation constant for fragment 1 on PS/POPC (10/90 mol/mol) membranes was $K_d \approx 8$ μM, which is equivalent to the previously published value. Approximately 20–25% of the fluorescence arose from protein in solution or nonspecifically bound to surface, as judged by measuring the evanescently excited fluorescence in the presence of EDTA. The binding of fragment 1 to DPPS/DPPC (10/90 mol/mol) planar membranes was examined at several protein concentrations. The results were similar to those for fragment 1 on PS/POPC membranes, with 20–25% of the fluorescence arising from protein in solution or nonspecifically bound to the surface.

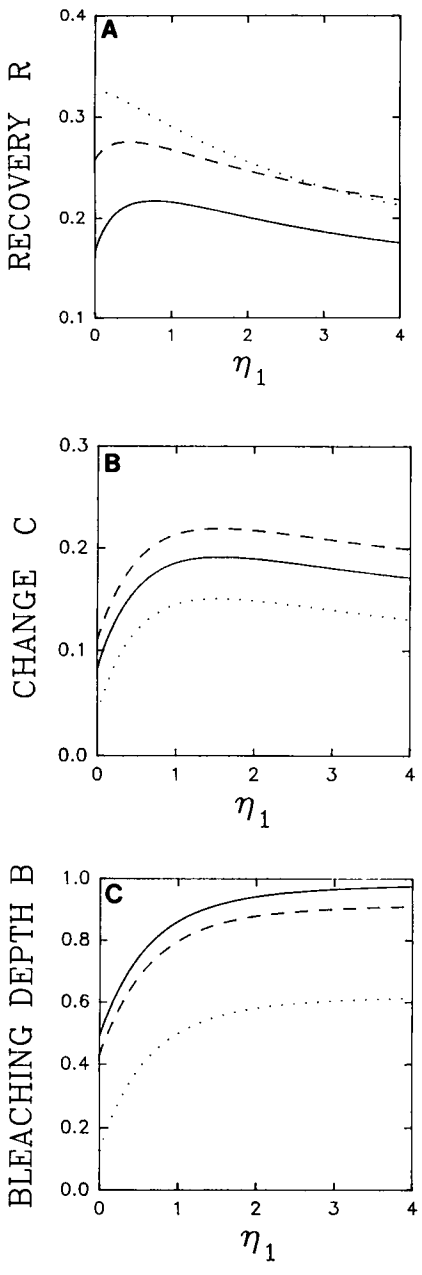

FIGURE 6 The fractional recovery R, the fractional fluorescence C, and the bleaching depth B as functions of the bleaching parameters η_1 and η_2. Values of (A) R, (B) C, and (C) B were calculated using Eqs. 6 and B1a and are shown for $V = 1$, $b = 0.5$, and $\eta_2 = 5$ (——), $\eta_2 = 1.5$ (-----), and $\eta_2 = 0.2$ (·····). The parameters V, b, and η_i are defined in Eqs. A1c, B4, and B6, respectively. R is maximized when η_1, $\eta_2 \to 0$, C is maximized when $\eta_1 \approx \eta_2 \approx 1.5$, and B is maximized when η_1, $\eta_2 \to \infty$.

Fragment 1 dissociation kinetics on fluid-like membranes measured by TIR-FPPR

TIR-FPPR data were obtained for fluorescein-labeled fragment 1 on fluid-like PS/POPC planar membranes, with one of the interfering beams blocked so that the bleaching and observation areas were large and elliptical in shape (Fig. 2 B). In these measurements, the laser intensity was increased twofold so that the fractional bleach was approximately equivalent to that measured for two interfering beams. The characteristic time for fluorescence recovery, which arose solely from the surface association/dissociation kinetics, was on the order of seconds, and nearly complete recovery occurred after a few minutes.

Previous work has demonstrated that, for large bleaching and observation areas where surface diffusion does not appreciably contribute to fluorescence recovery, the recovery curves are not monoexponential (Pearce et al., 1992, 1993). In this work, we consider two surface binding mechanisms that can account for the nonmonoexponential shapes of TIR-FPPR recovery curves for large areas. In one mechanism, fragment 1 isomerizes between two membrane-bound states, i.e.,

$$A + B \underset{k_{-1}}{\overset{k_1}{\rightleftharpoons}} C_1 \underset{k_{-2}}{\overset{k_2}{\rightleftharpoons}} C_2, \tag{7}$$

where A denotes protein in solution, B denotes unoccupied surface binding sites, C_1 and C_2 are membrane-bound complexes, and the k_i ($i = 1, -1, 2, -2$) are kinetic rate constants. In the other mechanism, there are two types of membrane sites to which fragment 1 binds, i.e.,

$$A + B_1 \underset{k_{-1}}{\overset{k_1}{\rightleftharpoons}} C_1 \qquad A + B_2 \underset{k_{-2}}{\overset{k_2}{\rightleftharpoons}} C_2, \tag{8}$$

where A denotes protein in solution, B_1 and B_2 denote unoccupied surface binding sites, C_1 and C_2 are membrane-bound complexes, and the k_i ($i = 1, -1, 2, -2$) are kinetic rate constants.

As shown in Appendix A, both mechanisms (Eqs. 7 and 8) give rise to biexponential recovery curves in the limit of large bleaching and observation areas. For the first mechanism,

$$G(t) = ge^{-\sigma_1 t} + (1 - g)e^{-\sigma_2 t} \tag{9}$$

where

$$2\sigma_{1,2} = \rho \pm \sqrt{\rho^2 - 4k_{-1}k_{-2}} \tag{10a}$$

$$\rho = k_{-1} + k_2 + k_{-2} \tag{10b}$$

$$g = \frac{\sigma_2 - fk_{-1}}{\sigma_2 - \sigma_1} \tag{10c}$$

$$f = \frac{k_{-2}}{k_2 + k_{-2}}. \tag{10d}$$

For the second mechanism,

$$G(t) = \gamma e^{-k_{-1}t} + (1 - \gamma)e^{-k_{-2}t} \tag{11a}$$

$$\gamma = \frac{(k_{-2} + k_2 A)k_1 \epsilon}{k_1 k_{-2}\epsilon + k_{-1}k_2(1 - \epsilon) + k_1 k_2 A}, \tag{11b}$$

where ϵ is the fraction of surface binding sites that are of the first type and γ is the fraction of *occupied* sites that are of the first type.

TABLE 1 Dissociation rates and fractional recoveries for fragment 1 on planar membranes

Type of membrane	A (μM)	r_1 (s^{-1})	a_1	r_2 (s^{-1})	a_2	$a_1 + a_2$
PS/POPC	2	2.69 ± 0.13	0.26 ± 0.01	0.25 ± 0.01	0.43 ± 0.01	0.69 ± 0.01
	4	2.83 ± 0.16	0.33 ± 0.01	0.31 ± 0.01	0.48 ± 0.01	0.81 ± 0.01
	8	3.18 ± 0.16	0.41 ± 0.01	0.37 ± 0.02	0.39 ± 0.01	0.80 ± 0.02
	20	3.89 ± 0.13	0.53 ± 0.01	0.45 ± 0.02	0.34 ± 0.01	0.88 ± 0.02
DPPS/DPPC	2	1.89 ± 0.21	0.33 ± 0.02	0.14 ± 0.02	0.21 ± 0.01	0.54 ± 0.03
	4	2.43 ± 0.20	0.38 ± 0.04	0.22 ± 0.02	0.22 ± 0.01	0.60 ± 0.04

Values were obtained from the best fits of control curves (large observation area data) to Eq. 12 and are the averages of 20–60 curves. r_1 and r_2 are the recovery rates, and a_1 and a_2 are the fractional recoveries associated with r_1 and r_2, respectively. Data were obtained with a sample interval of 10 ms, and fluorescence recovery was monitored for 12 s. Errors are SDs of the means.

Table 1 summarizes the kinetic data obtained by analyzing control curves (large observation area data). These data were fit to the theoretical form

$$F(t) = F(-) + [F(0) - F(-)][a_0 + a_1 e^{-r_1 t} + a_2 e^{-r_2 t}], \quad (12)$$

with $F(-)$ fixed at the known value, $a_0 = 1 - a_1 - a_2$, and with $F(0)$, a_1, a_2, r_1, and r_2 as free parameters. As shown in Table 1, both of the recovery rates and the fractional recoveries associated with the fast rate increased slightly with the fragment 1 solution concentration, and the fractional recoveries associated with the slow rate decreased slightly. The recovery rates are somewhat larger than those previously published (Pearce et al., 1992). A likely reason for this is that the data are not truly biexponential (Pearce et al., 1993), and the recovery curve data in this work were obtained with shorter time durations and therefore on a faster time scale.

For the two-step binding mechanism (Eq. 7), k_{-1}, k_2, and k_{-2} were calculated by using $\sigma_1 = r_1$, $\sigma_2 = r_2$, Eqs. 10, and the assumption that $g = a_1/(a_1 + a_2)$ (Pearce et al., 1992) (Table 2). For the two binding site type mechanism (Eq. 8), k_{-1}, k_{-2} and γ had the same values as σ_1, σ_2 and g. For the two-step binding mechanism, the rates k_{-1} and k_{-2} increased slightly with the fragment 1 solution concentration. The average rates were $k_{-1} \approx 3\ s^{-1}$ and $k_2 \approx k_{-2} \approx 0.3\ s^{-1}$. For the two binding site type mechanism, k_{-1}, k_{-2}, and (as expected) γ increased slightly with the fragment 1 solution concentration. The average dissociation rates were $\approx 3\ s^{-1}$ for one site type and $\approx 0.3\ s^{-1}$ for the other site type; the average value of γ was ≈ 0.5.

Protein translational diffusion on fluid-like membranes measured by TIR-FPPR

The translational diffusion of fragment 1 on fluid-like PS/POPC membranes was measured by obtaining TIR-FPPR recovery curves as a function of the pattern period P. As shown in Fig. 7 *A*, the rate of fluorescence recovery increased with decreasing P. In these measurements, the fluorescence recovery arose from both dissociation/association kinetics and protein surface translational diffusion, and the fractional recovery R was ≈ 1.

As shown in Appendix A, the shape of the fluorescence recovery for the two-step binding mechanism is

$$G(t) = [ge^{-\sigma_1 t} + (1 - g)e^{-\sigma_2 t}][(1 - h) + he^{-\sigma t}]. \quad (13)$$

Similarly, for the two-site binding mechanism,

$$G(t) = [\gamma e^{-k_{-1} t} + (1 - \gamma)e^{-k_{-2} t}][(1 - h) + he^{-\sigma t}]. \quad (14)$$

These equations apply when the diffusion coefficients of C_1 and C_2 are equal. TIR-FPPR data were fit to Eq. 1 with either Eq. 13 or 14; with $F(0)$, $F(-)$, h, and σ as free parameters, and with g, σ_1, σ_2, or γ, k_{-1}, k_{-2} fixed at the predetermined values (see above). The obtained rates σ were plotted versus $1/P^2$, and the data were fit by linear regression (Fig. 7 *B*). The protein translational diffusion coefficients D were obtained from the slopes (Eq. 3). Uncertainties in diffusion coefficients were calculated using linear regression theory (Taylor, 1982).

As shown in Fig. 7 *C*, the fragment 1 translational diffusion coefficients ranged from $(4.8 \pm 1.2) \times 10^{-9}$ cm^2/s for

TABLE 2 Kinetic rates for fragment 1 on planar membranes

Type of membrane	A (μM)	Two-step binding			Two binding site types		
		k_{-1}	k_{-2}	k_2	k_{-1}	k_{-2}	γ
PS/POPC	2	2.36 ± 0.16	0.28 ± 0.02	0.29 ± 0.04	2.69 ± 0.13	0.25 ± 0.01	0.38 ± 0.02
	4	2.49 ± 0.16	0.35 ± 0.02	0.30 ± 0.03	2.83 ± 0.16	0.31 ± 0.01	0.41 ± 0.02
	8	2.89 ± 0.25	0.41 ± 0.03	0.25 ± 0.01	3.18 ± 0.16	0.37 ± 0.02	0.51 ± 0.03
	20	3.64 ± 0.17	0.48 ± 0.03	0.22 ± 0.02	3.89 ± 0.13	0.45 ± 0.02	0.60 ± 0.03
DPPS/DPPC	2	1.81 ± 0.15	0.15 ± 0.01	0.073 ± 0.004	1.89 ± 0.21	0.14 ± 0.02	0.61 ± 0.03
	4	2.32 ± 0.10	0.23 ± 0.01	0.101 ± 0.009	2.43 ± 0.20	0.22 ± 0.02	0.63 ± 0.05

For the two-step binding mechanism (Eq. 7), the values of k_{-1}, k_{-2} and k_2 were calculated from the data in Table 1 by using $\sigma_1 = r_1$, $\sigma_2 = r_2$, Eqs. 10 and 14, and assuming that $g = a_1/(a_1 + a_2)$. For the two binding site type mechanism (Eq. 8), $k_{-1} = r_1$, $k_{-2} = r_2$ and $\gamma = a_1/(a_1 + a_2)$. The errors are SDs of the means.

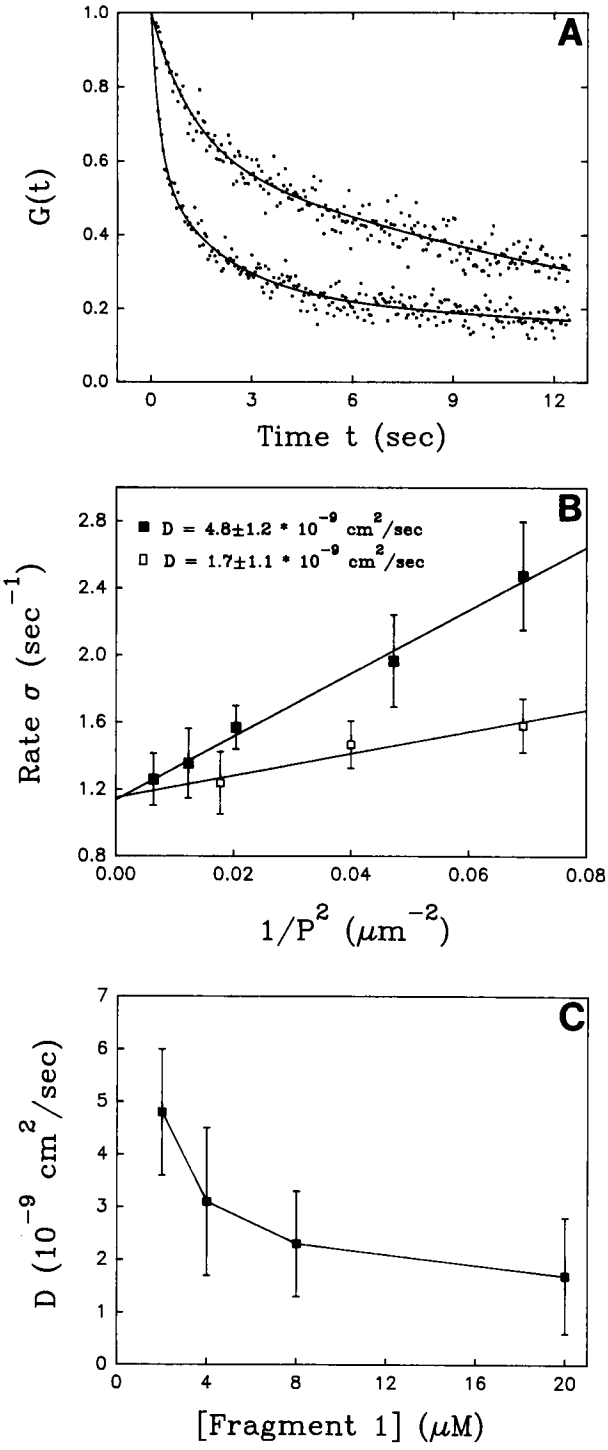

FIGURE 7 TIR-FPPR Data for fragment 1 on PS/POPC planar membranes. (*A*) Shown are typical curves for 2 μM fragment 1 on PS/POPC bilayers with 10 mM Ca^{2+} for a large observation area (*top*) and a pattern period of 7 μm (*bottom*). Decreasing the pattern period increases the rate of fluorescence recovery. The lines show the best fits to Eq. 13 (or Eq. 14). (*B*) Rates σ, obtained from the best fits of data like those in *A* to Eq. 13, are plotted as a function of $1/P^2$, where *P* is the fringe pattern period. Results are shown for 2 μM (■) and 20 μM (□) fragment 1. The error bars are SDs of the means. The slopes of the best fits to lines give diffusion coefficients. The uncertainties in the diffusion coefficients were calculated using linear regression. (*C*) The surface diffusion coefficients of fragment 1 are shown as a function of the fragment 1 solution concentration. Increasing the fragment 1 solution concentration decreases the surface diffusion coefficient.

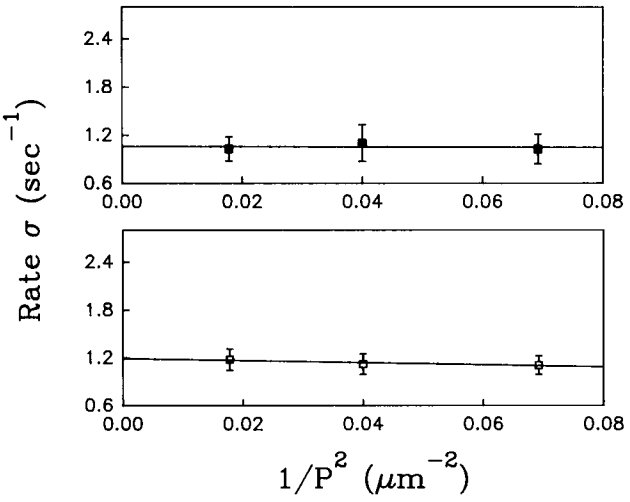

FIGURE 8 TIR-FPPR data for fragment 1 on DPPS/DPPC planar membranes. Rates σ, obtained from the best fits of data to Eq. 13 (or Eq. 14), are plotted as a function of $1/P^2$, where *P* is the fringe pattern period. Results are shown for 2 μM (■) and 4 μM (□) fragment 1. The error bars are SDs of the means. The data points were fit by linear regression. In both cases, the slopes were very low (and negative), indicating that there was no measurable protein translational mobility.

A = 2 μM (20% saturated) to (1.7 ± 1.1) × 10^{-9} cm^2/s for A = 20 μM (70% saturated). Two-tailed t-tests were carried out to evaluate the effects of the fragment 1 solution concentration on the surface diffusion coefficients. The values of p were as follows: $\ll$0.01 for comparing the diffusion coefficients for A = 2 and 4 μM; <0.01 for A = 4 and 8 μM; 0.0125 for A = 8 and 20 μM; and $\ll$0.001 for A = 2 and 20 μM. These results demonstrate that a significant reduction in the diffusion coefficient occurs with increasing protein solution concentration (and surface density).

Protein translational diffusion on solid-like membranes

As a control, TIR-FPPR data were obtained for fragment 1 on solid-like DPPS/DPPC membranes. Tables 1 and 2 list the kinetic rate constants obtained from the control curves (large observation area data). The fast recovery rates and the fractional recoveries associated with them were not significantly different from those on fluid-like PS/POPC membranes, whereas the slow rates, the fractional recoveries associated with them, and the total fluorescence recoveries differed somewhat. For the two-step binding mechanism, the values of k_{-1} were similar to those for fragment 1 on fluid-like membranes, whereas k_{-2} and k_2 were lower than those on fluid-like membranes. A possible reason for this difference is that the change in state associated with the second step depends on the lipid translational mobility, i.e., that the different membrane-bound states correspond to fragment 1 associated with different numbers of PS molecules. TIR-FPPR recovery curves obtained with fringe patterns were analyzed by the same method applied to the fluid-like membranes. As shown in Fig. 8, for both 2 and 4 μM fragment

1 solution concentrations, no recovery rate increases were found when decreasing the fringe pattern period. Thus, no protein translational mobility was detected.

Simulations of the effect of the fragment 1 solution diffusion on TIR-FPPR recovery curves

As shown in Table 2, increasing the protein solution concentration slightly increases the protein surface dissociation kinetic rates. This trend suggests that the system is not entirely reaction-limited, i.e., that the fluorescence is determined in part by the protein solution diffusion (Pearce et al., 1992). A potential artifact in the measurement of translational diffusion is that, if the system is not reaction-limited, decreasing the pattern period may increase the rate of fluorescence recovery even in the absence of surface diffusion because the system is being driven from a diffusion-limited case to a reaction-limited one (Thompson et al., 1981; Hsieh and Thompson, 1994). Thus, one might measure an artifactually high diffusion coefficient.

The general theoretical forms for TIR-FPPR, which account for solution diffusion, were used to evaluate its potential effect on the measurement of D (see Appendix C). In these calculations, the solution diffusion coefficient was $D_A = 5 \times 10^{-7}$ cm^2/s; the surface diffusion coefficient was $D = 4.8 \times 10^{-9}$ cm^2/s; the kinetic rate constants k_{-1}, k_2, and k_{-2} were equal to the values shown in Table 2 for 2 μM fragment 1 on PS/POPC membranes; the apparent surface dissociation constant was $K_d = 8$ μM; $\eta = V = 1$; and the total surface site density was $N = 26{,}500$ mol/μm^2 (Pearce et al., 1992). Fig. 9 *A* shows $G(t)$ as a function of the pattern period, as predicted by the general expression for the two-step binding mechanism (Eqs. C1–C5); Fig. 9 *B* shows $G(t)$ as predicted by the general expression for two binding site type mechanism (Eqs. C1 and C6–C8); and Fig. 9 *C* shows the dependence of $G(t)$ on the pattern period for the reaction-limited case as calculated from Eq. 13 (or 14). In all three cases, $G(t)$ decreases more rapidly with decreasing P. However, there is considerable difference between $G(t)$ for the general cases (Fig. 9, *A* and *B*) and for the reaction-limited

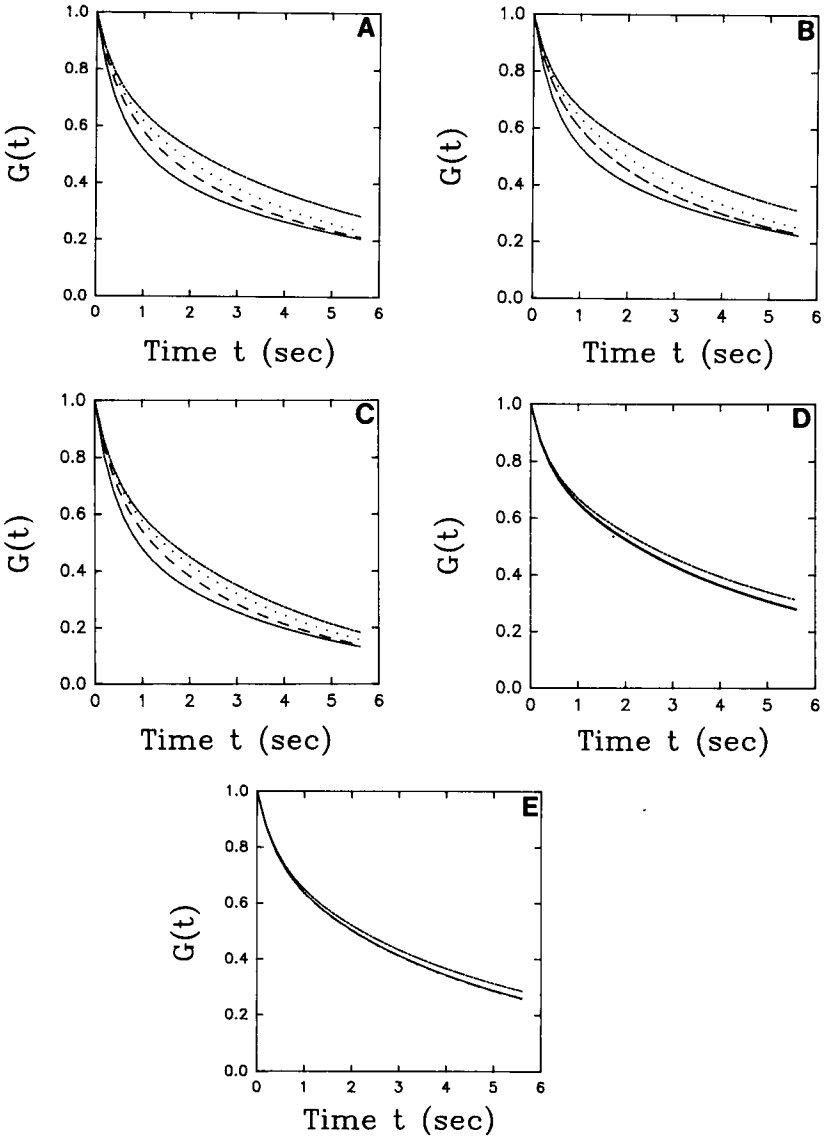

FIGURE 9 Theoretical values of $G(t)$. Results are shown for (*A*, *C*, *D*) the two-step binding mechanism (Eq. 7) and (*B*, *E*) the two binding site type mechanism (Eq. 8). $G(t)$ was calculated for $P = 4$ μm (——), 7 μm (– – –), 12.5 μm (· · · ·) and for a large observation area (·–·–·). The diffusion coefficients were $D_A = 5 \times 10^{-7}$ cm^2/s, and $D = 4.8 \times 10^{-9}$ cm^2/s, and $\eta = V = 1$. The values of (*A*, *C*, *D*) k_{-1}, k_2, and k_{-2} or (*B*, *E*) k_{-1}, k_{-2}, and γ were taken from Table 2 (2 μM, PS/POPC). $G(t)$ was calculated using (*A*, *B*) the general expressions (Eqs. C1–C8) and (*C*) the reaction-limited expressions (Eqs. 13 and 14) (the results are the same for two binding mechanisms). The values of $G(t)$ in *A*–*C* are considerably different, which means that the system is not predicted to be completely reaction-limited. (*D*, *E*) $G(t)$ was calculated with the same parameter values as for *A* and *B* except that $D = 0$.

case (Fig. 9 *C*), which means that the system is not completely reaction-limited. The above calculations were repeated assuming that surface diffusion coefficient D was zero and keeping all of the other parameters the same. In these cases, as shown in Fig. 9 *D* for the two-step binding mechanism and Fig. 9 *E* for the two binding site type mechanism, the values of $G(t)$ for different pattern periods overlapped whereas the $G(t)$ for a large observation area were somewhat different.

The simulated curves for $D = 0$ and 4.8×10^{-9} cm^2/s were analyzed using the same method as that used for experimental data to extract the surface translational diffusion coefficients (see above). Fig. 10 shows a plot of the best-fit values of σ vs. $1/P^2$ for (*A*) the two-step binding mechanism and (*B*) the two binding site mechanism. As shown, for $G(t)$ generated using $D = 0$, the analysis gives artificial diffusion coefficients of (*A*) $D = 1.7 \times 10^{-10}$ cm^2/s or (*B*) $D = 0.4 \times 10^{-10}$ cm^2/s. However, for $G(t)$ generated using $D = 4.8 \times 10^{-9}$ cm^2/s, the analysis procedure gives the correct values for D for both mechanisms. Therefore, although the experimental data are not completely in the reaction limit, the effect of the partial diffusion control on the measured value of D is negligible.

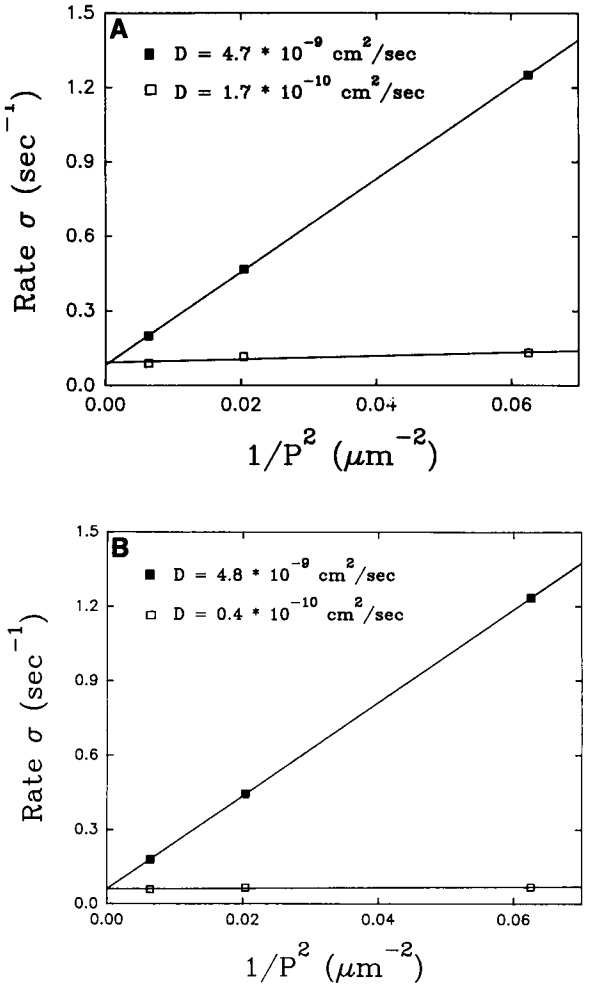

FIGURE 10 Diffusion coefficients as calculated from simulated data. The simulated curves in Fig. 9 *A*, *B*, *D*, and *E* were analyzed by the same method as that used for experimental data (see text). Shown in this figure are the best-fit values of the rates σ as functions of $1/P^2$, for (*A*) the two-step binding mechanism (Eq. 7) and (*B*) the two-binding site types mechanism (Eq. 8). As shown, for $G(t)$ generated using $D = 0$ (□), and (*A*) Eqs. C1–C5 or (*B*) Eqs. C1 and C6–C8, the analysis gives artifactual diffusion coefficients of (*A*) $D = 1.7 \times 10^{-10}$ cm^2/s or (*B*) $D = 0.4 \times 10^{-10}$ cm^2/s. However, for $G(t)$ generated using $D = 4.8 \times 10^{-9}$ cm^2/s (■), the analysis procedure gives the correct value for D. Therefore, although the experimental data are not completely in the reaction limit, the effect of the partial diffusion control on the measured value of D is negligible.

SUMMARY

The enzymatic conversion of prothrombin to the active serine protease, thrombin, is one of several membrane-mediated processes critically important in blood coagulation. This proenzyme activation involves an interplay between chemical reaction processes (protein-protein and protein-membrane interactions) and transport processes (surface translational/rotational diffusion, surface dissociation/association kinetics, protein solution diffusion). Among these processes, the surface diffusion of prothrombin is a key factor in understanding the interaction of prothrombin and the membrane-bound prothrombinase complex.

TIR-FPPR provides a new method for measuring the translational diffusion of proteins weakly bound to membrane surfaces. As compared with conventional FPPR, TIR-FPPR samples need not be restricted to a plane, in that the evanescent illumination allows discrimination between events at an interface from those that occur in bulk volume. This work represents the first successful measurement of the translational mobility of a protein weakly and specifically bound to a membrane surface.

The results described in this paper show that the lipid diffusion coefficient in fluid PS/PC planar membranes, as measured by TIR-FPPR, is $\approx 10^{-8}$ cm^2/s and matches well with the coefficient measured by conventional FPPR. Prothrombin fragment 1 bound to fluid-like PS/PC planar membranes at low surface densities has a diffusion coefficient $\approx 5 \times 10^{-9}$ cm^2/s. This value is approximately twofold lower than the lipid diffusion coefficient in the absence of bound fragment 1 and is approximately equivalent to the lipid diffusion coefficient in the presence of bound fragment 1 (Huang et al., 1992). In addition, no translational diffusion was detected for fragment 1 on solid-like PS/PC membranes. These results demonstrate that the translational diffusion of weakly bound fragment 1 requires and mimics membrane fluidity, which suggests that fragment 1 does not skim over the membrane surface. Because the limiting viscosity is that of the membrane, fragment 1 apparently remains bound to its lipid binding site throughout its surface occupancy. The fragment 1 surface diffusion coefficient is reduced approximately threefold when the fragment 1 surface density changes from 20 to 70% of the density at saturation. This result suggests that lateral protein-protein interactions significantly retard the fragment 1 surface diffusion when the fragment 1 surface density is high.

We thank Richard G. Hiskey of the University of North Carolina at Chapel Hill for assistance with fragment 1 preparations. This work was supported by National Institutes of Health grant GM-37145 (N. L. Thompson), National Science Foundation grant GER-9024028 (N. L. Thompson), and a Graduate Fellowship from the Hercules Corporation (K. H. Pearce).

APPENDIX A

TIR-FPPR recovery curves for combined surface diffusion and surface association/dissociation kinetics (reaction limit)

If the surface affinity and site density are high enough, the dominant signal in a TIR-FPPR experiment arises from molecules that are bound to the surface rather than in solution near the surface. In this case, the measured fluorescence is related to the evanescent intensity at the interface ($z = 0$). For two s-polarized, interfering beams with equal incidence angles and amplitudes, this intensity may be written in the form (Abney et al., 1992; Huang and Thompson, 1993)

$$I_{b,0}(y) = I^a_{b,0}[1 + V\cos(\beta y)] \tag{A1a}$$

$$\beta = \frac{4\pi n_q \sin\theta \sin\phi}{\lambda_0} \tag{A1b}$$

$$V = |\cos 2\phi|. \tag{A1c}$$

$I_0(y)$ is the evanescent intensity used for fluorescence monitoring, $I_b(y)$ is the evanescent intensity used for fluorescence bleaching, $I^a_{b,0}$ are the spatially averaged intensities, β is the spatial periodicity, λ_0 is the vacuum wavelength of the incident beam, n_q is the refractive index of the quartz, θ is the incidence angle, ϕ is the semi-angle of intersection of the two interfering beams, V is the visibility, and the relationship between β and the period of the interference pattern, P, is shown in Eq. 3b. In the measurements described herein, $\lambda_0 = 488.0$ nm, $n_q = 1.47$, $\theta \approx 75°$, $\phi = 0.7°$–$2.5°$, $P \approx 4$–15 μm, and $V \approx 1$.

The time-dependent fluorescence recovery $F(t)$ after photobleaching may be written as

$$F(t) = Q\int_0^P I_0(y)S(y, t)\,dy, \tag{A2}$$

where $S(y, t)$ is the surface concentration of unbleached fluorescent molecules at time t and position y, and Q is a proportionality constant. Eq. A2 is based on the assumption that the fluorophore absorption dipoles are isotropically oriented and homogeneously distributed. The equation also neglects the (often small) effects of the nearby planar dielectric interface on the angular dependence of the fluorescence emission and the influence of the microscope collection optics on the fluorescence collection efficiency.

For a simple, monovalent binding mechanism (Abney et al., 1992)

$$A + B \underset{k_{-1}}{\overset{k_1}{\rightleftharpoons}} S, \tag{A3}$$

where A is the solution concentration of fluorophores, B is the surface density of unoccupied surface sites, and S is the two-dimensional density of surface-bound fluorophores. In the reaction limit, the fluorescence recovery depends on both the surface association/dissociation kinetic rates and the surface diffusion coefficient. The differential equation governing $S(y, t)$ is

$$\frac{\partial}{\partial t}S(y, t) = D\frac{\partial^2}{\partial y^2}S(y, t) + k_1[A(y, z, t)]_{z\to 0}B(y, t) - k_{-1}S(y, t), \tag{A4}$$

where z is the distance from the interface and y lies in the sample plane and is perpendicular to the fringe stripes; A, B, and S are functions of both space and time; and D is the surface diffusion coefficient of S. For photobleaching measurements, $B(y, t)$ is a constant (Thompson et al., 1981); and, in the reaction limit, $[A(y, z, t)]_{z\to 0}$ is also a constant (see Appendix C). The initial condition is

$$S(y, 0) = \langle S\rangle e^{-\kappa I_b(y)} \approx \langle S\rangle[1 - \kappa I_b(y)], \tag{A5}$$

where κ is a parameter proportional to the bleaching duration and efficiency, $I_b(y)$ is the bleaching beam intensity, and the approximation holds in the limit of shallow bleaching. $\langle S\rangle$ is the equilibrium concentration of $S(y, t)$. The differential equation may be solved by using Fourier transform methods. Substituting the obtained $S(y, t)$ into Eq. A2 and using Eq. 1, one finds that

$$G(t) = e^{-k_{-1}t}[(1 - h) + he^{-\sigma t}], \tag{A6}$$

where h and σ are defined in Eqs. 3c and 3a, and

$$\eta = \kappa I^a_b. \tag{A7}$$

When $k_{-1} = 0$, the fluorescence recovery arises purely from surface diffusion, and $G(t)$ reduces to a one-exponential form with characteristic rate σ (Eq. 2). When $\sigma\to 0$,

$$G(t) = e^{-k_{-1}t}, \tag{A8}$$

which represents reaction-limited, monovalent dissociation kinetics for a large observation area (Thompson et al., 1981).

The differential equations for the mechanism shown in Eq. 7 are

$$\frac{\partial}{\partial t}C_1(y, t) = D_1\frac{\partial^2}{\partial y^2}C_1(y, t) + k_1[A(y, z, t)]_{z\to 0}B(y, t) - (k_{-1} + k_2)C_1(y, t) + k_{-2}C_2(y, t) \tag{A9a}$$

$$\frac{\partial}{\partial t}C_2(y, t) = D_2\frac{\partial^2}{\partial y^2}C_2(y, t) + k_2C_1(y, t) - k_{-2}C_2(y, t), \tag{A9b}$$

where C_1 and C_2 are functions of both space and time, and D_1 and D_2 are the protein surface diffusion coefficients for the different bound states. In the reaction limit, $[A(y, z, t)]_{z\to 0}$ and $B(y, t)$ are constants. The initial conditions are

$$C_1(y, 0) = \langle C_1\rangle\exp^{-\kappa I_b(y)} \approx \langle C_1\rangle[1 - \kappa I_b(y)] \tag{A10a}$$

$$C_2(y, 0) = \langle C_2\rangle\exp^{-\kappa I_b(y)} \approx \langle C_2\rangle[1 - \kappa I_b(y)], \tag{A10b}$$

where κ and $I_b(y)$ are defined above, and the approximation holds in the limit of shallow bleaching. $\langle C_1\rangle$ and $\langle C_2\rangle$ are the equilibrium concentrations of $C_1(y, t)$ and $C_2(y, t)$, and are related by $k_2\langle C_1\rangle = k_{-2}\langle C_2\rangle$.

The differential equations in Eqs. A9 may be solved by using Fourier transform methods. Substituting $S(y, t) = C_1(y, t) + C_2(y, t)$ into Eqs. A2 and 1, one finds that

$$G(t) = \sum_{i-1}^{4} h_i e^{-\sigma_i t}, \tag{A11}$$

where $\sigma_{1,2}$ are defined in Eq. 10a,

$$2\sigma_{3,4} = (D_1 + D_2)\beta^2 + \rho \pm \sqrt{f(\beta)} \tag{A12a}$$

$$h_{1,2} = \pm(1 - h)\frac{\sigma_{2,1} - fk_{-1}}{\sigma_2 - \sigma_1} \tag{A12b}$$

$$h_{3,4} = \pm h\frac{\sigma_{4,3} - [fk_{-1} + fD_1\beta^2 + (1 - f)D_2\beta^2]}{\sigma_4 - \sigma_3} \tag{A12c}$$

$$f(\beta) = [(D_1 - D_2)\beta^2 + (k_{-1} + k_2 - k_{-2})]^2 + 4k_2k_{-2}, \tag{A12d}$$

and β, h, and f are defined above (Eqs. 3b, 3c, and 10d). When $D_1 = D_2 = D$, $G(t)$ reduces to Eq. 13. For a large observation area ($\sigma \to 0$), Eqs. A11 and 13 reduce to the previously published form (Eq. 9) (Pearce et al., 1992). For irreversibly adsorbed molecules ($k_{-1} \to 0$), $\sigma_{1,2} \to 0$, and Eq. 13 reduces to Eq. 2. When the second membrane-bound state is not abundantly occupied ($k_2/k_{-2} \to 0$), $g \to 1$, $\sigma_1 \to k_{-1}$, and Eqs. A11 and 13 reduce to Eq. A6 (the form for monovalent binding).

For the mechanism shown in Eq. 8, we assume that the sites are independent, so that

$$F_i(t) = F_i(-) + [F_i(0) - F_i(-)]G_i(t), \tag{A13}$$

where $i = 1$ or 2, $F_i(t)$ is the fluorescence associated with molecules bound to the ith site type, and $G_i(t)$ is defined above (Eq. 1). The

measured fluorescence $F(t)$ is the sum of $F_1(t)$ and $F_2(t)$. By using Eqs. 1 and A13 with

$$F(t) = F_1(t) + F_2(t) \tag{A14a}$$

$$\gamma = \frac{F_1(-) - F_1(0)}{F(-) - F(0)}, \tag{A14b}$$

where γ is the fraction of occupied surface binding sites that are of the first type, one finds that

$$G(t) = \gamma G_1(t) + (1 - \gamma)G_2(t) \tag{A15}$$

$$= \gamma e^{-k_{-1}t}[(1 - h) + he^{-D_1\beta^2 t}] + (1 - \gamma)e^{-k_{-2}t}[(1 - h) + he^{-D_2\beta^2 t}].$$

In the limit of a large observation area ($\beta \to 0$), Eq. A15 reduces to Eq. 11. If we assume that the two types of surface-bound complexes have the same translational diffusion coefficients, or $D_1 = D_2 = D$, then Eq. A15 reduces to Eq. 14. If, in addition, $k_{-1} = k_{-2} \to 0$, Eq. A15 reduces to Eq. 2. When $\gamma = 1$, Eq. A15 reduces to Eq. A6.

In all three surface-binding mechanisms, $G(t)$ separates into distinct surface diffusion and chemical kinetic factors (Eqs. 13, 14, and A6). In addition, the mechanisms shown in Eqs. 7 and 8 generate different recovery rates, but both have a biexponential form in the limit of a large observation area.

In general, TIR-FPPR fluorescence recovery curves depend not only on the surface association/dissociation kinetic rates and surface diffusion coefficients, but also on the solution diffusion coefficient (Thompson et al., 1981; Hsieh and Thompson, 1994). The results shown in this Appendix are applicable to the reaction limit of TIR-FPPR, in which solution diffusion is rapid and/or the solution concentration is high. The more general case is described in Appendix C.

APPENDIX B

Fractional recoveries *R* and fractional fluorescence changes *C* in the absence of surface association/dissociation

The fractional recovery R may be defined in terms of the fractional fluorescence change C and the fractional bleach B, i.e.,

$$R = \frac{F(\infty) - F(0)}{F(-) - (F(0)} = 1 - G(\infty) = \frac{C}{B} \tag{B1a}$$

$$C = \frac{F(\infty) - F(0)}{F(-)} \tag{B1b}$$

$$B = \frac{F(-) - F(0)}{F(-)}. \tag{B1c}$$

By using the expression for $F(t)$ (Appendix A), one finds the dependence of R, B, and C on η and V (Eqs. 4) for irreversibly bound fluorophores.

The possibility exists that the bleaching and observation beam interference patterns might be shifted in phase. Following the methods of derivation outlined in Appendix A, with

$$I_o(y) = I_o^a[1 + V\cos(\beta y + \xi)], \tag{B2}$$

where ξ is the phase shift, one finds that

$$\frac{F(t)}{F(-)} = Z_0(\eta, V) - Z_1(\eta, V)e^{-\beta^2 Dt}\cos(\xi), \tag{B3}$$

where the Z_i are defined in Eq. 3d. Eq. B3 implies Eqs. 5.

Another possibility is that the bleaching process is not exponential, i.e.,

$$S(y, 0) = \langle S\rangle[be^{-\kappa_1 I_b(y)} + (1 - b)e^{-\kappa_2 I_b(y)}], \tag{B4}$$

where $0 \le b \le 1$ is a constant and $\kappa_1 \ne \kappa_2$. This equation implies that

$$\frac{F(t)}{F(-)} = [bZ_0(\eta_1, V) + (1 - b)Z_0(\eta_2, V)] - [bZ_1(\eta_1, V) + (1 - b)Z_1(\eta_2, V)]e^{-\beta^2 Dt}, \tag{B5}$$

where the Z_i are defined in Eq. 3d and

$$\eta_i = \kappa_i I_b^a. \tag{B6}$$

Eq. B5 implies Eqs. 6.

APPENDIX C

Effect of solution diffusion on TIR-FPPR recovery curves

The results shown in Appendix A are applicable to the reaction-limit of TIR-FPPR. The general result is given by (Hsieh and Thompson, 1994)

$$G(t) = (1 - h)H(0, t) + hH(\beta, t), \tag{C1}$$

where h is given in Eq. 3c and $H(\beta, t)$ depends on the membrane-binding mechanism.

For membrane binding according to the two-step mechanism (Eq. 7) with $D_1 = D_2 = D$, the function $H(\beta, t)$ is given by (Hsieh and Thompson, 1994)

$$H(\beta, t) = \sum_{i=1}^{5} A_i\sqrt{\alpha_i}e^{(\alpha_i - \beta^2 D_A)t}\operatorname{erfc}(-\sqrt{\alpha_i t}), \tag{C2}$$

where D_A is the protein diffusion coefficient in solution,

$$A_i = \frac{\sum_{n=0}^{3} c_n \alpha_i^{n/2}}{(\sqrt{\alpha_i} - \sqrt{\alpha_j})(\sqrt{\alpha_i} - \sqrt{\alpha_k})(\sqrt{\alpha_i} - \sqrt{\alpha_l})(\sqrt{\alpha_i} - \sqrt{\alpha_m})}, \tag{C3}$$

the $\sqrt{\alpha_{i,j,k,l,m}}$ are the five roots of

$$\left[\sqrt{\alpha} + \frac{fk_{-1}}{\sqrt{R}}\right] \times [\{\alpha + k_{-2} + (D - D_A)\beta^2\}\{\alpha + k_2 + k_{-1} + (D - D_A)\beta^2\} - k_2 k_{-2}] - \frac{k_{-1}^2 f}{\sqrt{R}}[\alpha + k_{-2} + (D - D_A)\beta^2] = 0 \tag{C4}$$

and

$$c_0 = \frac{fk_{-1}}{\sqrt{R}}[k_2 + k_{-2} + (D - D_A)\beta^2] \tag{C5a}$$

$$c_1 = k_2 + k_{-2} + (D - D_A)\beta^2 + (1 - f)k_{-1} \tag{C5b}$$

$$c_2 = \frac{fk_{-1}}{\sqrt{R}} \tag{C5c}$$

$$c_3 = 1 \tag{C5d}$$

$$R = \frac{D_A(fk_{-1} + k_1 A)^2}{(Nk_1)^2}, \tag{C5e}$$

and f is defined in Eq. 10d, N is the total density of surface binding sites. This general expression reduces to the reaction-limited case (Eq. 13) when $k_{-1} \ll R$.

For membrane binding according to the two binding site type mechanism, the function $H(\beta, t)$ is given by (Thompson et al., 1981)

$$H(\beta, t) \tag{C6}$$

$$= \sum_{i=1}^{3}\left\{\gamma \frac{\sqrt{\alpha_{i1}}[\sqrt{\alpha_{i1}} + k_{-1}/\sqrt{R_1}]}{[\sqrt{\alpha_{i1}} - \sqrt{\alpha_{j1}}][\sqrt{\alpha_{i1}} - \sqrt{\alpha_{ki}}]} e^{[(\alpha_{i1} - \beta^2 D_A)t]} \operatorname{erfc}(-\sqrt{\alpha_{i1}}t)\right.$$

$$\left. + (1-\gamma)\frac{\sqrt{\alpha_{i2}}[\sqrt{\alpha_{i2}} + k_{-2}/\sqrt{R_2}]}{[\sqrt{\alpha_{i2}} - \sqrt{\alpha_{j2}}][\sqrt{\alpha_{i2}} - \sqrt{\alpha_{k2}}]} e^{[(\alpha_{i2} - \beta^2 D_A)t]} \operatorname{erfc}(-\sqrt{\alpha_{i2}}t)\right\},$$

where the $\sqrt{\alpha_{im}}$, $\sqrt{\alpha_{jm}}$, and $\sqrt{\alpha_{km}}$ (for $m = 1$ or 2) are the three roots of

$$\left[\sqrt{\alpha} + \frac{k_{-m}}{\sqrt{R_m}}\right][\alpha + k_{-m} + (D - D_A)\beta^2] - \frac{k_{-m}^2}{\sqrt{R_m}} = 0 \tag{C7}$$

and

$$R_m = D_A\left(\frac{(K_d + A}{N_m}\right)^2 \tag{C8}$$

γ is defined in Eq. A14, K_d is the equilibrium dissociation constant (which is assumed to be equivalent for both site types), and N_m is the total surface density of sites of type m, for $m = 1$ or 2. This general expression reduces to the reaction-limited case (Eq. 14) when $k_{-1} \ll R$.

REFERENCES

Abbott, A. J., and G. L. Nelsestuen. 1988. The collisional limit: an important consideration for membrane-associated enzymes and receptors. *FASEB J.* 2:2858–2866.

Abney, J. R., B. A. Scalettar, and N. L. Thompson. 1992. Evanescent interference patterns for fluorescence microscopy. *Biophys. J.* 61:542–552.

Hsieh, H. V., and N. L. Thompson. 1994. Theory for measuring bivalent surface binding kinetics using total internal reflection with fluorescence photobleaching recovery. *Biophys. J.* 66:898–911.

Huang, Z., K. H. Pearce, and N. L. Thompson. 1992. Effect of bovine prothrombin fragment 1 on the translational diffusion of phospholipids in Langmuir-Blodgett monolayers. *Biochim. Biophys. Acta.* 1112:259–265.

Huang, Z., and N. L. Thompson. 1993. Theory for two-photon excitation in pattern photobleaching with evanescent illumination. *Biophys. Chem.* 47:241–249.

Jackson, C. M., and Y. Nemerson. 1980. Blood coagulation. *Annu. Rev. Biochem.* 49:765–811.

Kalb E., S. Frey, and L. K. Tamm. 1992. Formation of supported planar bilayers by fusion of vesicles to supported phospholipid monolayers. *Biochim. Biophys. Acta.* 1103:307–317.

Mann, K. G., M. E. Nesheim, W. R. Church, P. Haley, S. Krishnaswamy. 1990. Surface dependent reactions of the vitamin K-dependent enzyme complexes. *Blood.* 76:1–16.

Miehlich, R., and H. E. Gaub. 1993. Holographic pattern photobleaching apparatus for the measurement of the lateral transport processes at interfaces—design and performance. *Rev. Sci. Instrum.* 64:2632–2638.

Pearce, K. H., R. G. Hiskey, and N. L. Thompson. 1992. Surface binding kinetics of prothrombin fragment 1 on planar membranes measured by total internal reflection fluorescence microscopy. *Biochemistry.* 31:5983–5995.

Pearce, K. H., M. Hof, B. R. Lentz, and N. L. Thompson. 1993. Comparison of the membrane binding kinetics of bovine prothrombin and its fragment 1. *J. Biol. Chem.* 268:22984–22991.

Smith, B. A., and H. M. McConnell. 1978. Determination of molecular motion in membranes using periodic pattern photobleaching. *Proc. Natl. Acad. Sci. USA.* 75:2759–2763.

Taylor, J. R. 1982. An introduction to error analysis. The Study of Uncertainties in Physical Measurements. D. Commins, editor. Oxford University Press.

Tendian, S. W., B. R. Lentz, and N. L. Thompson. 1991. Evidence from total internal reflection fluorescence microscopy for calcium-independent binding of prothrombin to negatively charged planar phospholipid membranes. *Biochemistry.* 30:10991–10999.

Thompson, N. L., Z. Huang, D. Gesty, and E. C. Bowles. 1994. Dynamics of proteins on supported planar membranes: measurement by total internal reflection fluorescence microscopy. *In* Current Topics in Biophysics. U. J. Krull and D. P. Nikolelis, editors. Iasi University Press, Romania. In press.

Thompson, N. L., T. P. Burghardt, and D. Axelrod. 1981. Measuring surface dynamics of biomolecules by total internal reflection fluorescence with photobleaching recovery or correlation spectroscopy. *Biophys. J.* 33: 435–454.

Thompson, N. L., K. H. Pearce, and H. V. Hsieh. 1993b. Total internal reflection fluorescence microscopy: application to substrate-supported planar membranes. *Eur. Biophys. J.* 22:367–378.

Thompson, N. L., C. L. Poglitsch, M. M. Timbs, and M. L. Pisarchick. 1993a. Dynamics of antibodies on planar model membranes. *Accts. Chem. Res.* 26:567–573.

Tilton, R. D., A. P. Gast, C. R. Robertson. 1990b. Surface diffusion of interacting proteins. Effect of concentration on the lateral mobility of adsorbed bovine serum albumin. *Biophys. J.* 58:1321–1326.

Tilton, R. D., C. R. Robertson, and A. P. Gast. 1990a. Lateral diffusion of bovine serum albumin adsorbed at the solid-liquid interface. *J. Colloid Interface Sci.* 137:192–203.

Weis, R. M., K. Balakrishnan, B. A. Smith, and H. M. McConnell. 1982. Stimulation of fluorescence in a small contact region between rat basophil leukemia cells and planar lipid membrane targets by coherent evanescent radiation. *J. Biol. Chem.* 257:6440–6445.

Wright, L. L., A. G. Palmer, and N. L. Thompson. 1988. Inhomogeneous translational diffusion of monoclonal antibodies on phospholipid Langmuir-Blodgett films. *Biophys. J.* 54:463–470.